Letters

Enhanced Maximum Power Point Reaching Method for Passive Magnetic Energy Harvesters Operating Under Low Primary Currents

Alexander Abramovitz, Moshe Shvartsas, and Alon Kuperman, *Senior Member, IEEE*

***Abstract*—The letter concerns a clamped-type passive magnetic energy harvester (MEH), supplying power to a general load via a diode bridge rectifier (DBR). It is known that a certain value of output MEH voltage (referred to as optimal) maximizes harvested power. Under high primary current magnitudes, the optimal voltage value is constant, i.e., current-independent. Consequently, it was recently proposed to interface a passive MEH to a general load via a switching power converter whose input (i.e., MEH-side) voltage is regulated to a corresponding constant voltage reference, realizing the maximum power point reaching (MPPR) method. However, optimal voltage value becomes current-dependent under low primary current magnitudes. As a result, the power harvested by MPPR-operated MEH becomes suboptimal if the MEH-side voltage reference of the converter remains unchanged. Hence, the brief suggests allowing the converter input voltage reference value to be adjusted (by, e.g., a maximum power point tracking loop) to maximize harvested MEH power under low primary currents as well. Experimental results comparing the harvested power of a passive MEH under classical and enhanced MPPR methods validate the proposed enhancement.**

***Index Terms*—Constant voltage load, diode bridge rectifier, magnetic energy harvester, maximum power point.**

I. Introduction

MAGNETIC energy harvesters (MEHs) clamped on ac-current-carrying conductor allow convenient powering of devices operating at low dc voltage [1], [2] via a suitable power electronics interface [3]. Passive MEHs utilize diode bridge rectifiers (DBRs) for rectification, offering simplicity and enhanced reliability [4]. It was shown in [5] that the power harvested by a passive MEH is maximized under a certain (optimal) value of output (dc-side) voltage. Moreover, if the MEH operates under primary current magnitudes much higher than the core saturation current, the optimal value of the output MEH voltage becomes constant (i.e., does not change when the primary current magnitude varies) [6]. In order to exploit this characteristic while feeding a general load, it was proposed in [7] to insert a switching power converter between MEH output and the load and regulate its MEH-side voltage to a constant value, which is optimal under high primary currents. As a result, the load is decoupled from the MEH and harvested power is permanently maximized under high primary currents [8]. Such an approach was entitled as maximum power point reaching (MPPR). Unfortunately, the optimal value of output MEH voltage becomes current-dependent, yielding suboptimal harvested power of MPPR-operated MEH under low primary currents [4], [7]. It then becomes clear that the MEH-side voltage reference value of the converter should be adjusted to allow harvested power maximization under low primary currents. Consequently, this brief quantifies the influence of low primary currents on the optimal value of output MEH voltage and suggests employing an additional control loop (feedforward or feedback) capable of adjusting the MEH-side voltage reference value of an MPPR-operated converter. Such an approach is often used in photovoltaic generators, where an external maximum power point tracking (MPPT) loop drives the inner voltage loop [9], [10]. A use case is discussed, indicating ∼14% increase in harvested MEH power under $20A_{rms}$ primary current with the proposed enhancement.

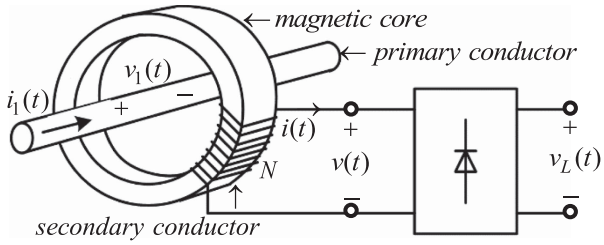

Fig. 1. MEH under consideration.

II. System Under Consideration

Passive MEH depicted in Fig. 1 is considered hereafter, comprising a current transformer clamped on a conductor carrying current $i_1(t)$. The MEH feeds a dc load via DBR. The load is assumed to impose the voltage $v_L(t)$ across dc-side MEH terminals. The equivalent circuit of the current transformer (reflected on the secondary side) is shown in Fig. 2. Under sinusoidal primary current $i_1(\theta) = I_1 \sin\theta$ with $\theta = \omega t$ and ω signifying system base angular frequency, its secondary side reflection is

Manuscript received 29 January 2024; revised 21 February 2024; accepted 9 March 2024. Date of publication 12 March 2024; date of current version 19 April 2024. *(Corresponding author: Alon Kuperman.)*

The authors are with Applied Energy Laboratory, School of Electrical and Computer Engineering, Ben-Gurion University of the Negev, Beer-Sheva 8410501, Israel (e-mail: alonk@bgu.ac.il).

Color versions of one or more figures in this article are available at https://doi.org/10.1109/TPEL.2024.3376540.

Digital Object Identifier 10.1109/TPEL.2024.3376540

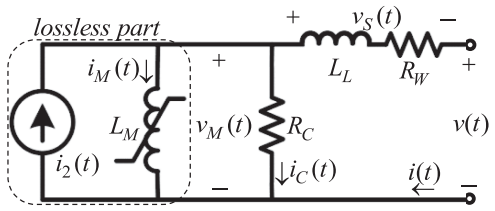

Fig. 2. Transformer equivalent circuit (reflected to the secondary side).

given by

$$i_2(\theta) = N^{-1} i_1(\theta) = I_2 \sin(\theta), \quad I_2 = N^{-1} I_1 \tag{1}$$

with I_1 and I_2 denoting primary and reflected currents magnitudes, respectively; N standing for the number of secondary transformer conductor turns. Referring to Fig. 2, L_M and L_L symbolize magnetizing and leakage transformer inductances; R_C and R_W denote equivalent core loss and secondary conductor resistances, respectively; core magnetizing voltage and current are titled $v_M(t)$ and $i_M(t)$, while terminal voltage and current of the secondary transformer conductor are represented by $v(t)$ and $i(t)$, respectively.

Voltage induced across the primary conductor [denoted by $v_1(t)$, cf., Fig. 1] is linked to magnetizing core voltage as

$$v_1(\theta) = N^{-1} v_M(\theta). \tag{2}$$

Hence, instantaneous power p_{in} harvested by the MEH from the current carrying conductor is given by

$$p_{\text{in}}(\theta) = v_1(\theta) i_1(\theta) = v_M(\theta) i_2(\theta). \tag{3}$$

Output impedance of the transformer (formed by series connection of leakage inductance and wire resistance) is assumed sufficiently low while core resistance is presumed sufficiently high for

$$v'_L(t) = v_L(t) + V_R >> |v_S(t)|, i_C(t) << i(t) \tag{4}$$

to hold with v'_L defining the modified load voltage, V_R denoting the voltage drop across two conducting rectifier diodes, i_C signifying the current flowing through R_C and v_S denoting the voltage drop across transformer output impedance. The circuit in Fig. 2 may then be accurately reduced to "lossless part" only.

III. MPPR by a Passive MEH

Piecewise linear core B-H curve is adopted with magnetic flux density B and magnetic field strength H linked as [11]

$$B = \begin{cases} \mu H, & |H| \le H_{\text{SAT}} \\ \text{sgn}(H) B_{\text{SAT}}, & |H| \ge H_{\text{SAT}} \end{cases}, \tag{5}$$

were μ, H_{SAT}, and B_{SAT} denote the initial core permeability and saturation values of magnetic H and B, respectively. Magnetic field strength is proportional to core magnetizing current as

$$H(\theta) = l_C^{-1} N i_M(\theta) \tag{6}$$

with l_C titling mean magnetic flux path length of the core. Saturation value of magnetizing current $I_{M,\text{SAT}}$ is defined as

$$I_{M,\text{SAT}} = l_C N^{-1} H_{\text{SAT}}. \tag{7}$$

Passive MEH operation assuming that (4) is valid and the primary current magnitude is sufficiently high for

$$I_1 >> N I_{M,\text{SAT}} \tag{8}$$

to hold was analyzed in [11] as follows. There are two operational DBR states during the half mains cycle given by $\theta_1 \le \theta \le \theta_1 + \pi$.

1) DBR is ON (conducting) within $\theta_1 \le \theta \le \theta_2$ interval (referred to as "transfer window" [5]), delivering energy to the load. During this state $v_M \approx v'_L$, hence, the magnetic flux density rises from $B(\theta_1) = -B_{\text{SAT}}$ to $B(\theta_2) = +B_{\text{SAT}}$.
2) DBR is OFF (not conducting) within $\theta_2 \le \theta \le \theta_1 + \pi$ interval and no energy is delivered to the load. $v_M \approx 0$ is assumed here, hence, the magnetic flux density is constant, i.e., $B(\theta_1 + \pi) = B(\theta_2) = +B_{\text{SAT}}$.

Instants θ_1 and θ_2 were found in [11] as

$$\theta_1 = -\sin^{-1}\left(N I_{M,\text{SAT}} I_1^{-1}\right) \approx 0 \tag{9}$$

and

$$\theta_2 = \theta_1 + \Delta\theta \approx \Delta\theta, \quad \Delta\theta = 2 B_{\text{SAT}} \omega N A_C (v'_L)^{-1} \tag{10}$$

respectively, with A_C designating the cross-sectional area of the core and $\Delta\theta$ defining the transfer window length. Corresponding average harvested MEH power is then given by [cf., (3), (5), (9), (10)]

$$\begin{aligned} P_{\text{in}} &= \pi^{-1} \int_{\theta_1}^{\theta_2} v_M(\theta) i_2(\theta) d\theta \approx (\pi N)^{-1} v'_L I_1 \int_0^{\Delta\theta} \sin\theta d\theta \\ &= (\pi N)^{-1} v'_L I_1 \left(\sin(\theta_1)\sin(\Delta\theta) \right. \\ &\quad \left. + \cos(\theta_1)(1 - \cos(\Delta\theta))\right) \\ &\approx 2\pi^{-1} \omega B_{\text{SAT}} A_C I_1 \underbrace{(1 - \cos(\Delta\theta))(\Delta\theta)^{-1}}_{f(\Delta\theta)} \\ &= \frac{2 f(\Delta\theta)}{\pi} \omega B_{\text{SAT}} A_C I_1 \end{aligned} \tag{11}$$

maximized at

$$\Delta\theta = \Delta\theta^* \approx 2.33 \text{ rad} \tag{12}$$

as

$$f(\Delta\theta^*) = 0.724 \Rightarrow P_{\text{in}}^* = P_{\text{in}}(\Delta\theta^*) \approx 0.46 \omega B_{\text{SAT}} A_C I_1. \tag{13}$$

Combining (10) with (12), optimal modified load voltage value

$$\begin{aligned} (v'_L)^*(t) = (v'_L)^* &= 2 B_{\text{SAT}} \omega N A_C (\Delta\theta^*)^{-1} \\ &\approx 0.858 B_{\text{SAT}} \omega N A_C \end{aligned} \tag{14}$$

is constant and current-independent. Hence, it was proposed in [7] to insert a switching power converter whose input terminals voltage is regulated to a constant reference $V_L^* = (V'_L)^* - V_R$ between passive MEH output and general load. A corresponding functional diagram is shown in Fig. 3, demonstrating the MPPR concept. Here, a constant voltage value V_L^* is imposed at MEH output irrespective of actual general load characteristics, implying harvested MEH power maximization under assumption (5).

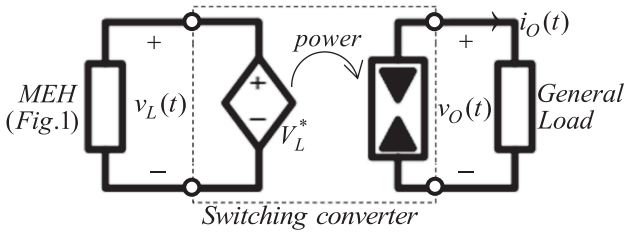

Fig. 3. Functional diagram of MPPR concept.

IV. MPPR Concept Under Low Primary Currents

Substitution of (5) into (14) yields

$$I_1 >> \frac{(v'_L)^* I_{M,\mathrm{SAT}}}{0.858\omega A_C B_{\mathrm{SAT}}}. \tag{15}$$

Since the value of A_C is set according to the desired amount of power to be harvested [cf., (13)], while the value of l_C is bounded by the area required to accommodate primary and secondary conductors, none of the variables forming the right-side hand expression in (15) may be freely selected by a designer. Consequently, (5) would not hold for low values of I_1. Moreover, the realistic B-H curve of the core material is nonlinear and is described more accurately by [12]

$$B = \frac{2}{\pi} B_{\mathrm{SAT}} \arctan(\mu H) = \frac{2}{\pi} B_{\mathrm{SAT}} \arctan\left(\mu l_C^{-1} N i_M\right). \tag{16}$$

This implies that at the end of DBR conducting state, $B(\theta_2) = k_2 B_{\mathrm{SAT}}$ in general with $k_2 < 1$ [as opposed to $k_2 \equiv 1$ when (5) and (6) are assumed]. Likewise, magnetizing voltage

$$v(\theta) = N A_C dB(\theta)/d\theta > 0 \tag{17}$$

is nonzero during DBR OFF state so that magnetic flux density reduces [since $i_M(\theta) = i_2(\theta)$ cf., (16)] rather than remains constant, i.e., $B(\theta_1+\pi) = k_1 B_{\mathrm{SAT}} < B(\theta_2)$ with $k_1 < k_2$ [as opposed to $k_1 \equiv 1$ when (5) and (6) are assumed]. Therefore, magnetic flux density rises during DBR conduction state from $B(\theta_1) = -B(\theta_1+\pi) = -k_1 B_{\mathrm{SAT}}$ to $B(\theta_2) = k_2 B_{\mathrm{SAT}}$ so that the actual transfer window length

$$\begin{aligned}\Delta\theta &= (k_1 + k_2) B_{\mathrm{SAT}} \omega N A_C \left((v'_L)^*\right)^{-1} \\ &= \frac{k_1 + k_2}{2} \Delta\theta^* < \Delta\theta^*\end{aligned} \tag{18}$$

is lower than the one expected in (12). Actual average harvested MEH power is then given by

$$\begin{aligned}P_{\mathrm{in}} \approx \pi^{-1} (k_1 + k_2) f\left(\Delta\theta = \frac{k_1 + k_2}{2}\Delta\theta^*\right) \\ \times \omega B_{\mathrm{SAT}} A_C I_1 < P_{\mathrm{in}}^*.\end{aligned} \tag{19}$$

Note that k_1 and k_2 decrease when I_1 reduces [cf., (16)]. It is evident that the actual average harvested MEH power is lower than the one expected in (13). The ratio between actual (19) and expected (13) power values is given by

$$\frac{P_{\mathrm{in}}}{P_{in}^*} \approx \alpha f_n, \quad \alpha = \frac{k_1 + k_2}{2}, \quad f_n = \frac{f(\Delta\theta = \alpha\Delta\theta)}{f(\Delta\theta = \Delta\theta^*)} \tag{20}$$

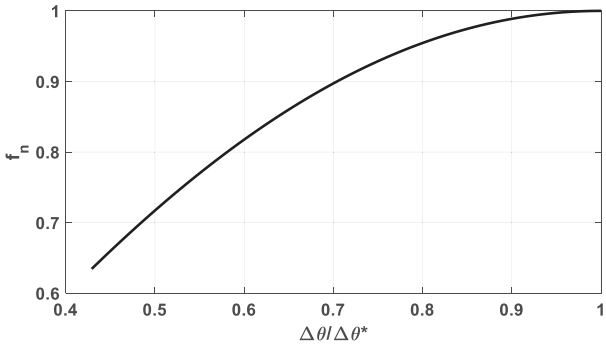

Fig. 4. Values of f_n versus normalized transfer window length.

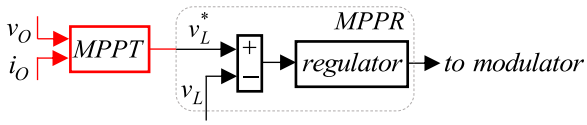

Fig. 5. Control structure of classical and MPPT-enhanced MPPR concept.

reducing with the decrease of I_1. Moreover, $f_n < 1$ (cf., Fig. 4) for any k_1, $k_2 < 1$, i.e., the value of modified load voltage in (14) is suboptimal when (5) does not hold. This phenomena was noticed in both [4] and [7].

V. Enhancing the MPPR Concept

Since k_1 and k_2 depend on the primary current magnitude, it is impossible to manipulate their values. On the other hand, it is possible to increase the transfer window length by reducing the value of v_L so that the argument of $f(\cdot)$ in (20) is forced to (12), i.e.,

$$\alpha\Delta\theta = 2.33 \tag{21}$$

so that $f_n = 1$ is attained bringing (20) to

$$P_{\mathrm{in}}/P_{\mathrm{in}}^* \approx \alpha \tag{22}$$

i.e., harvested MEH power would be increased by $0.724/f(2.33\alpha)$ compared to classical MPPR method. The required value of v_L is [cf., (10)]

$$v_L^* = \frac{k_1 + k_2}{2.33} B_{SAT} \omega N A_C - V_R. \tag{23}$$

Adjustment of v_L may be carried out by either online calculation of k_1 and k_2 (which requires sensing/estimation of I_1) or employing an additional MPPT loop, as shown in Fig. 5.

Unfortunately, the ratio between actual and expected power values (20) is much more sensitive to the value of α (the sensitivity is unity) than to that of f_n (the sensitivity is much less than unity, cf., Fig. 4). Thus, the proposed enhancement is expected to increase the harvested MEH power only under low primary currents.

VI. Experimental Verification

Consider an MEH comprising a transformer based on a silicon steel core ($B_{\mathrm{SAT}} \approx 2$ T) with $N = 60$ secondary conductor turns,

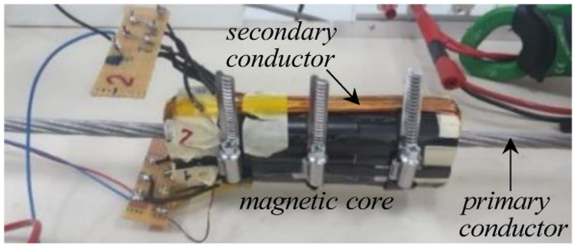

Fig. 6. Experimental MEH transformer.

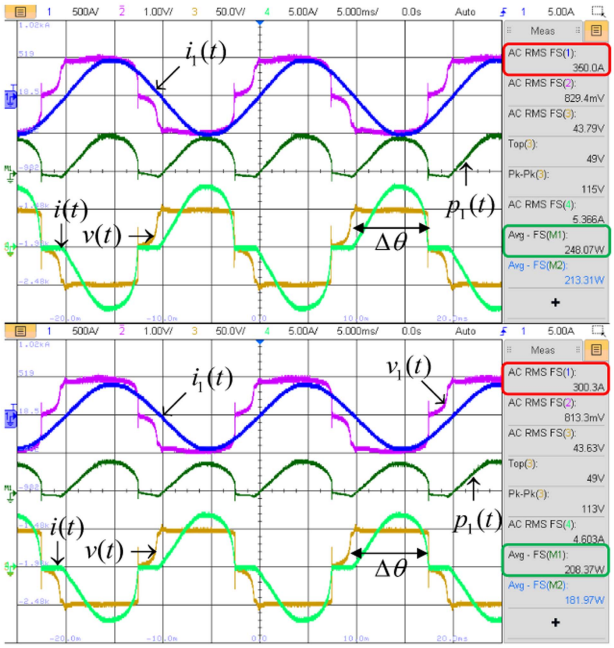

Fig. 7. MEH performance under high primary currents, MPPR.

a cross-sectional area of $A_C = 1.8{\cdot}10^{-3}$ m^2, and mean magnetic flux path length of $l_C = 0.12$ m. for accommodating primary and secondary conductors. A prototype transformer is depicted in Fig. 6.

SB256 module ($V_R \approx 2$ V) is employed as DBR and the MEH is terminated by M9715B Maynuo dc electronic load, operated in CV mode at $V_L = 45$ V. During experiments, voltage induced across the primary conductor and corresponding current were measured along with transformer terminal voltage and current. Under primary currents of 300 A_{rms}@50 Hz and above, amounts of harvested MEH power were maximized at $V_L = 45$ V and accurately matched (13) with

$$P_{in}\left(I_{1,\text{rms}} \geq 300A, V_L = 45V\right) \approx 0.7 I_{1,\text{rms}} = P_{\text{in}}^{*}. \quad (24)$$

Moreover, transfer window lengths are 0.75π as expected by (12) (see Fig. 7). Under moderate primary currents (below 300 A_{rms} yet above 75 A_{rms}), amounts of harvested MEH power deviate from (24) so that (cf., Fig. 8)

$$\begin{aligned} P_{\text{in}}\left(I_{1,\text{rms}} = 250A, V_L = 45V\right) &\approx 0.67 I_{1,\text{rms}} < P_{\text{in}}^{*} \\ P_{\text{in}}\left(I_{1,\text{rms}} = 100A, V_L = 45V\right) &\approx 0.58 I_{1,\text{rms}} < P_{\text{in}}^{*} \end{aligned} \quad (25)$$

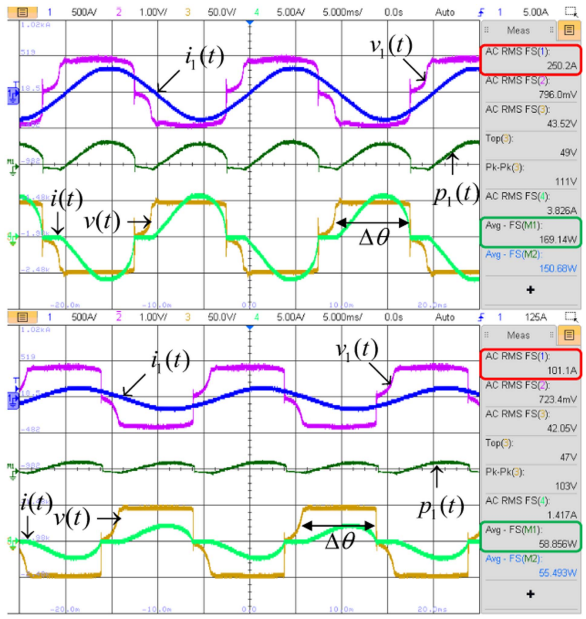

Fig. 8. MEH performance under moderate primary currents, MPPR.

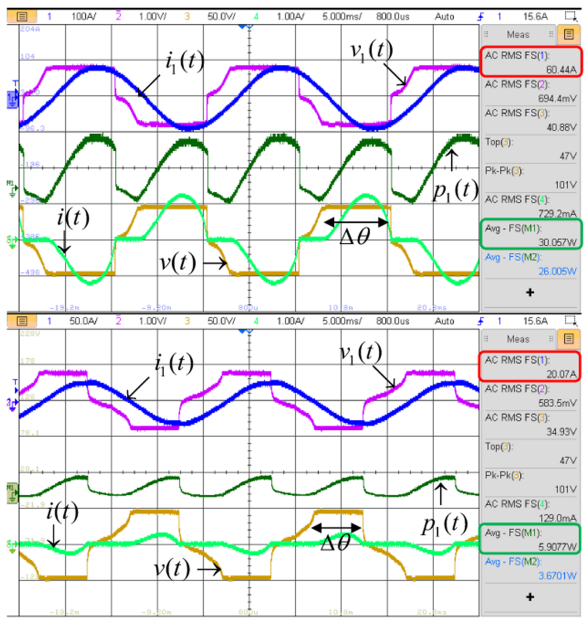

Fig. 9. MEH performance under low primary currents, MPPR.

while still maximized at $V_L = 45$ V. Corresponding transfer window lengths are slightly below $\sim 0.75\pi$, as expected. Yet, it is nearly impossible to increase the harvested power in this region of primary currents due to the low sensitivity of f_n in the vicinity of $\Delta\theta = 0.75\pi$ (cf., Fig. 4).

Under low primary currents (below 75 A_{rms}), amounts of harvested MEH power both deviated from (24) at $V_L = 45$ V so that (cf., Fig. 9)

$$\begin{aligned} P_{\text{in}}\left(I_{1,\text{rms}} = 60A, V_L = 45V\right) &\approx 0.497 I_{1,\text{rms}} << P_{\text{in}}^{*} \\ P_{\text{in}}\left(I_{1,\text{rms}} = 20A, V_L = 45V\right) &\approx 0.294 I_{1,\text{rms}} << P_{\text{in}}^{*}. \end{aligned} \quad (26)$$

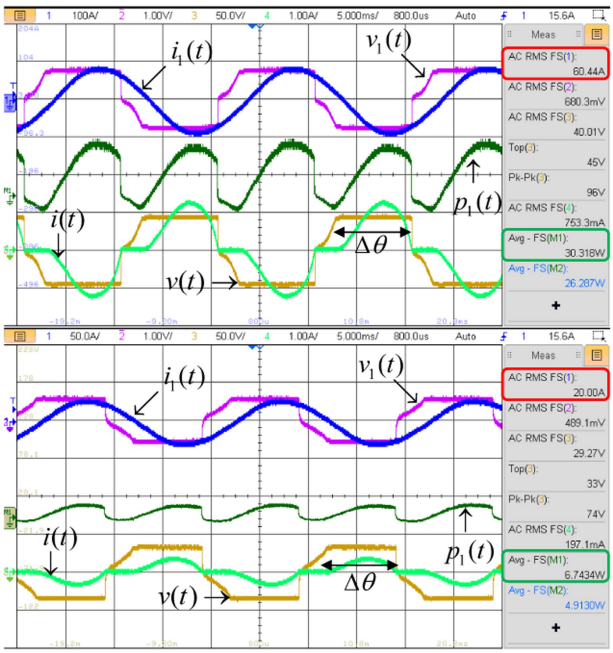

Fig. 10. MEH performance under low primary currents, MPPT+MPPR.

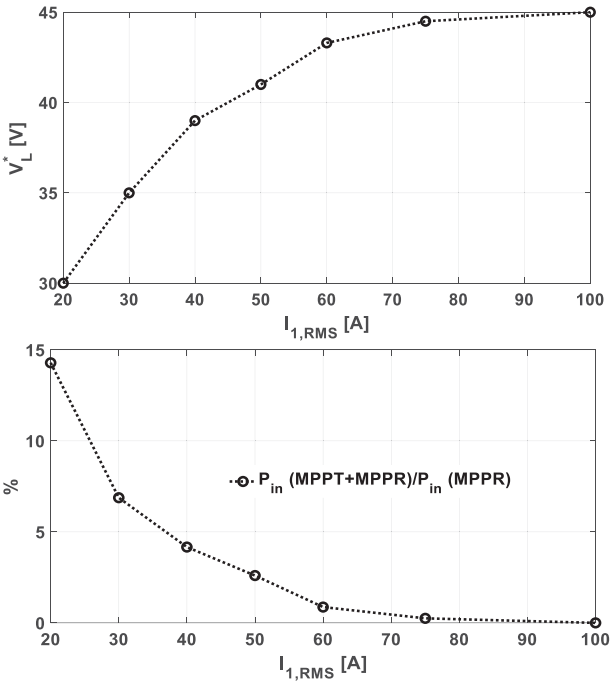

Fig. 11. Optimal load voltage (top) and percentage harvested MEH power increase under low primary currents.

Moreover, it is clear that the corresponding transfer window lengths are well below 0.75π. Consequently, there is some potential for increased harvested power in this region of primary currents by adjusting V_L. Thus, the electronic load voltage was varied under each primary current to obtain the value maximizing harvested MEH power. As a result, (26) was enhanced as (cf., Fig. 10)

$$P_{\text{in}}\left(I_{1,\text{rms}}=60A, V_L=43.5V\right) \approx 0.502 I_{1,\text{rms}} << P_{\text{in}}^*$$
$$P_{\text{in}}\left(I_{1,\text{rms}}=20A, V_L=30V\right) \approx 0.337 I_{1,\text{rms}} << P_{\text{in}}^* \quad (27)$$

demonstrating 1.1% and 14.3% harvesting power increase under primary currents of 60 A_{rms} and 20 A_{rms}, respectively. And optimal transfer window lengths are restored. The results are summarized in Fig. 11. It is concluded that under low primary currents, nonnegligible relative increase of harvested MEH power may be attained by the proposed enhancement at the expense of additional sensors (if not present) and MPPT loop implementation. On the other hand, in the case of a simple low-cost analog MPPR realization as in [7], such an enhancement may not be worthwhile.

VII. Conclusion

This letter quantified the harvested MEH power increase attained by utilizing an additional loop with the MPPR method. In case the MEH operates under high and moderate primary currents, the proposed method would be inefficient. On the other hand, it was revealed that up to 14% (for the presented case) increase may be attained under low primary currents.

References

[1] Z. Liu, Y. Li, N. Duan, and Z. He, "An energy management method for magnetic field energy harvesters under wide-range current in railway electrification systems," *IEEE Trans. Ind. Electron.*, vol. 71, no. 5, pp. 5360–5369, May 2024.

[2] D. Monagle, E. A. Ponce, and S. B. Leeb, "Rule the joule: An energy management design guide for self-powered sensors," *IEEE Sensors J.*, vol. 24, no. 1, pp. 6–15, Jan. 2024.

[3] T. Suntio, J. Viinamäki, J. Jokipii, T. Messo, and A. Kuperman, "Dynamic characterization of power electronic interfaces," *IEEE J. Emerg. Sel. Topics Power Electron.*, vol. 2, no. 4, pp. 949–961, Dec. 2014.

[4] A. Abramovitz, M. Shvartsas, and A. Kuperman, "On the maximum power of passive magnetic energy harvesters feeding constant voltage loads under high primary currents," *IEEE Trans. Power Electron.*, to be published, doi: 10.1109/TPEL.2024.3350348.

[5] J. Moon and S. B. Leeb, "Analysis model for magnetic energy harvesters," *IEEE Trans. Power Electron.*, vol. 30, no. 8, pp. 4302–4311, Aug. 2015.

[6] D. Monagle, E. Ponce, and S. B. Leeb, "Generalized analysis method for magnetic energy harvesters," *IEEE Trans. Power Electron.*, vol. 37, no. 12, pp. 15764–15773, Dec. 2022.

[7] K. Ye et al., "A novel method of maximum power point reaching for magnetic field energy harvesting based on a low-power analog control circuit," *IEEE Trans. Power Electron.*, vol. 39, no. 1, pp. 1888–1897, Jan. 2024.

[8] A. Kuperman, M. Averbukh, and S. Lineykin, "Maximum power point matching versus maximum power point tracking for solar generators," *Renewable Sustain. Energy Rev.*, vol. 19, pp. 11–17, Mar. 2013.

[9] S. Kolesnik et al., "Solar irradiation independent expression for photovoltaic generator maximum power line," *IEEE J. Photovolt.*, vol. 7, no. 5, pp. 1416–1420, Sep. 2017.

[10] J. Kivimäki, S. Kolesnik, M. Sitbon, T. Suntio, and A. Kuperman, "Design guidelines for multi-loop perturbative maximum power point tracking algorithms," *IEEE Trans. Power Electron.*, vol. 33, no. 2, pp. 1284–1293, Feb. 2018.

[11] Z. Liu, Y. Li, H. Yang, N. Duan, and Z. He, "An accurate model of MEH in the saturated region for harvesting maximum power: Analysis, design and experimental verification," *IEEE Trans. Ind. Electron.*, vol. 70, no. 1, pp. 276–285, Jan. 2023.

[12] M. J. Vos, "A magnetic core permeance model for inductive power harvesting," *IEEE Trans. Power Electron.*, vol. 35, no. 4, pp. 3627–3635, Apr. 2020.